

Non-triangular potential sweep cyclic voltammetry of reversible electron transfer: Experiment meets theory

Hatem M.A. Amin, Yuki Uchida, Christopher Batchelor-McAuley, Enno Kätelhön and Richard G. Compton*

* Corresponding author: Richard G. Compton

Department of Chemistry, Physical & Theoretical Chemistry Laboratory, University of Oxford, South Parks Road, Oxford, OX1 3QZ, United Kingdom

Email: richard.compton@chem.ox.ac.uk. Tel: +44(0)1865275 957 Fax: +44(0)1865275410

Abstract

Conventionally, cyclic voltammetry is performed using triangular waveforms; however, complications can arise from the discontinuity of the capacitive current at the potential vertex in the triangular wave. Recent literature (J. Electroanal. Chem. 2017, 801, 381-387) showed theoretically the opportunities offered by non-triangular waveforms. Herein, we test this theory for the reversible aqueous system $[\text{Ru}(\text{NH}_3)_6]^{3+/2+}$ using cosine-based waves at a glassy carbon macroelectrode. The match between the theoretical and experimental results is excellent and offers an alternative and novel method to determine the formal potential E_f° of the $\text{Ru}^{3+}/\text{Ru}^{2+}$ system. The scan rate dependency of the voltammograms is investigated; and for the cosine wave voltammetry the peak currents are 24% higher than that obtained from the typical triangular waves, coinciding with the simulation results.

Keywords: Cyclic voltammetry; Non-triangular waveform; Reversible reaction; Hexamineruthenium(III) chloride

1. Introduction

In electroanalytical chemistry, cyclic voltammetry is the most frequently used technique because it offers a wealth of analytical, kinetic, thermodynamic and mechanistic information on many chemical systems resulting in concentrations, rate constants and formal potentials [1-4]. A typical cyclic voltammogram involves varying the potential of the working electrode with time. The current at the working electrode is recorded as a function of the applied potential $E(t)$. In cyclic voltammetry CV, the measured current is the sum of the faradaic and capacitive currents. The capacitive contribution appears ideally as a rectangular in the voltammograms and its current is proportional to the scan rate. The great progress in the theoretical understanding of this technique led to quantitative analysis of complex systems including porous electrodes and adsorbed species [4-6].

Characterisation of the reactive intermediates and obtaining experimental data in the nanosecond time scale are challenging. Therefore, ultrafast cyclic voltammetry was used to offer a timescale compatible with higher electron transfer rates [7-10].

The sensitivity of a voltammetric measurement is limited by the ratio of faradaic to capacitive currents. Therefore, a correction for capacitive currents I_c is generally required in particular when I_c is either not constant or is large as in ultrafast cyclic voltammetry [9, 10]. Although modern techniques including impedance spectroscopy, pulse voltammetry [11] and AC voltammetry have been widely used to quantitatively analyse electron transfer processes and to discriminate the capacitive currents [12], they still have some limitations as for instance AC voltammetry [13, 14] requires a significantly more complex analysis procedure than cyclic voltammetry.

In spite of the advantages and simplicity of the triangular wave cyclic voltammetry, complications arise from the discontinuity of the capacitive currents at the potential vertex of the wave. Such discontinuity can generate perturbations in the voltammetric data especially at high scan rates. This issue can be reduced by employing a different waveform in which the temporal gradient of the applied potential $\partial E_i(t)$ is continuous. Alternative potential waveforms [15] based on the cosine function have recently been introduced by Uchida et al., who simulated and analysed the cosine-based voltammograms for an electrochemically-reversible reaction. They discussed the unique features in the simulated voltammograms that can be exploited to determine the formal potential. Kätelhön et al. extended this later through a theoretical treatment of adsorbed species [16].

In this paper, we present an experimental verification of the theory suggested by Uchida et al. [15] for the reversible $\text{Ru}^{3+}/\text{Ru}^{2+}$ system. Hence, the triangular, cosine and cosine square potential waveforms were applied at a GC macroelectrode in an aqueous solution of $[\text{Ru}(\text{NH}_3)_6]\text{Cl}_3$. Successful

experimental validation of the theoretical results is realized. Analysis of the peak currents shows an excellent agreement with the simulated currents. Finally, the peak-to-peak separations revealed a unique feature (i.e. jump in the potential at a certain E_{centre} value) that is utilized as a novel method to determine the formal potential of this redox couple. The measured formal potential is consistent with that obtained from other independent methods.

2. Theoretical Model

In this section we summarize the theory underlying the voltammetry of a reversible one-electron transfer process. We investigate a solution containing an electroactive species $[Ru(NH_3)_6]^{3+}$ that undergoes a reversible electrochemical reduction to $[Ru(NH_3)_6]^{2+}$ [17, 18] at a planar macroelectrode under diffusion-only conditions so that the solution is assumed to be fully supported to suppress migration: [17]



In this fully “reversible” system, the electrode kinetics are *fast* compared to the mass transport rate such that the Nernstian equilibrium is attained at the electrode surface throughout: [2, 3]

$$E = E_f^0 + \frac{RT}{F} \ln \frac{[Ru^{3+}]_{x=0}}{[Ru^{2+}]_{x=0}} \quad (2)$$

where E is the applied potential and $x=0$ denotes the position at zero distance from surface. E_f^0 is the formal potential of Ru^{3+}/Ru^{2+} couple.

In the triangular wave cyclic voltammetry, the potential of the working electrode $E(t)$ changes linearly relative to a reference electrode, which maintains a constant potential:

$$E(t) = \begin{cases} E(t=0) \pm vt & \text{for } t < \frac{1}{2}t_{cycle} \\ E\left(t = \frac{1}{2}t_{cycle}\right) \mp v\left(t - \frac{1}{2}t_{cycle}\right) & \text{for } t \geq \frac{1}{2}t_{cycle} \end{cases} \quad (3)$$

where $E(t=0)$ is the initial potential, t_{cycle} is the duration of a single cycle between the two potential limits and v is the scan rate.

In contrast to the conventional triangular wave, Uchida et al. has recently introduced an alternative potential wave based on a cosine function [15] which is simplified as follows:

$$E(\tau) = A_0 \cdot |\cos(2\pi\tau)|^{n-1} \cdot \cos(2\pi\tau) + E_{centre} \quad (4)$$

$$\tau = \frac{t}{t_{cycle}} \quad (5)$$

$$E_{centre} = \frac{E_f - E_i}{2} \quad (6)$$

where A_0 is the amplitude of the wave (here is 0.45 V) and E_{centre} is the midpoint potential of the applied potential window which is experimentally defined relative to the reference electrode. E_i is the start potential and E_f is the vertex potential. When $n=1$, a simple *cosine* potential wave is applied and for $n=2$ a *cosine square* wave is employed. The shapes of the triangular, cosine and cosine square potential waves that are experimentally conducted are shown in Fig. 1. In all waves, the duration of a single cycle is kept the same for the applied potential window so that the scan rate averaged over the potential cycle for the non-triangular wave is the same as that in the triangular one, but the instantaneous scan rate varies during the cycle depending on the applied potential for the non-triangular voltammetry, see Fig. 1. Most notably, for the cosine square wave a plateau corresponding to a temporary zero scan rate is observed at E_{centre} of the applied potential window.

In practice, the position of this plateau E_{centre} is moved up and down in terms of the potential at which it is applied by shifting the potential window. The non-triangular waveforms also have the property that the first temporal derivative of the potential is continuous so that $\partial E_t(\tau)$ of Eq. (4) is a continuous function. In this way, the capacitive current discontinuity at the potential vertex is avoided.

The simulations were performed using two different methods, namely the finite difference approach [19] and the fractional calculus method [20], which were implemented in C++: Details of both are described elsewhere [15].

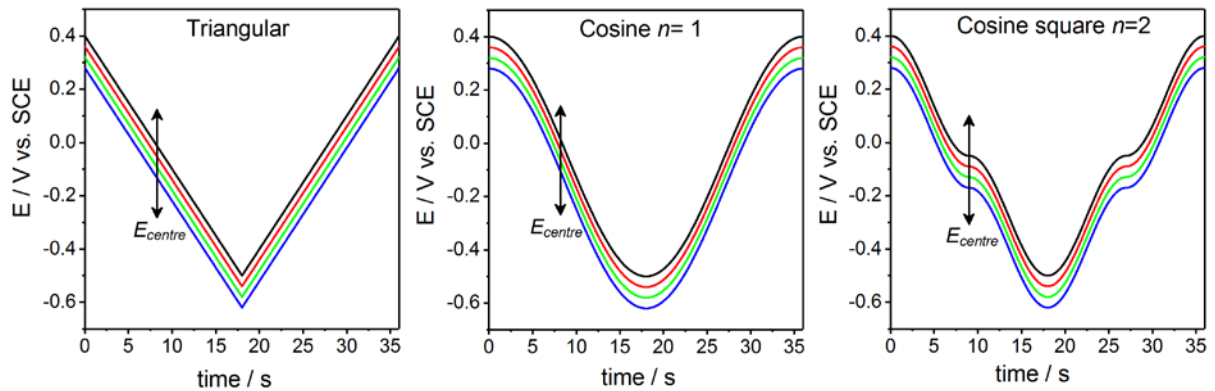


Fig. 1. The triangular and cosine-based waveforms (for $n=1$ or 2) applied in this work at different potential windows (i.e. E_{centre} shifts up and down in the potential scale for the different potential windows).

3. Experimental Section

Hexaammineruthenium(III) chloride ($[\text{Ru}(\text{NH}_3)_6]\text{Cl}_3$, 98%, Aldrich) and potassium chloride (Aldrich, >99%) were used as received without further purification. All solutions were prepared with Milli-Q water with resistivity not less than $18.2 \text{ M}\Omega \text{ cm}^{-1}$ at 298 K (Millipore Water Systems, UK) and degassed for 30 min with N_2 (99.998%, BOC, U.K.) prior each experiment and over solution during the measurement.

All voltammetry experiments were carried out with an in-house built potentiostat controlled through a computer, as described previously elsewhere [21]. The potentiostat was controlled through a script written in Python 3.5 to generate the required potential waveform (Fig. 1). A graphical user interface for data visualisation was provided in the Enthought Canopy package (Enthought, TX). The working electrode was controlled by a highly stabilized potentiostat (2 kHz bandwidth), where the potential of the working electrode is nominally controlled in intervals of 60 μV . A USB-6003 DAQs (National Instruments, TX) was used for digital-to-analog and analog-to-digital conversion. Data collection was achieved using the Python software, and the plots were drawn using OriginPro 2017. A low current-amplifier DLPCA-200 (Femto Messtechnik GmbH, Berlin, Germany) was used to measure the current at the working electrode and the bandwidth of the output of the current amplifier was limited using two cascaded 2 kHz passive RC-filters. The resulting analog signal was oversampled at a stream rate of 100 kHz.

Before the application of each potential wave, the working electrode was held at the start potential for 3 s. A three-electrode setup was employed, with a glassy carbon (GC, 3.0 mm diameter, ALS Co. Ltd, Japan) disc as working electrode, a saturated calomel electrode (SCE, ALS Co. Ltd, Japan) reference electrode and a Pt wire (GoodFellow, Cambridge, U.K.) as the counter electrode. Prior experiments, the GC electrode was polished with MicroPolish alumina (Buehler, IL, U.S.A.) slurry onto soft lapping pads (Buehler, U.S.A.) of decreasing size (1, 0.3 and 0.05 μm), followed by ultrasonic treatment in acetone bath for 1 min, then in deionized water for 1 min and finally dried under nitrogen flow.

The temperature was maintained constant at 298 K using a water bath connected to a temperature controller (SCT1, Stuart, U.K.) in a Faraday cage.

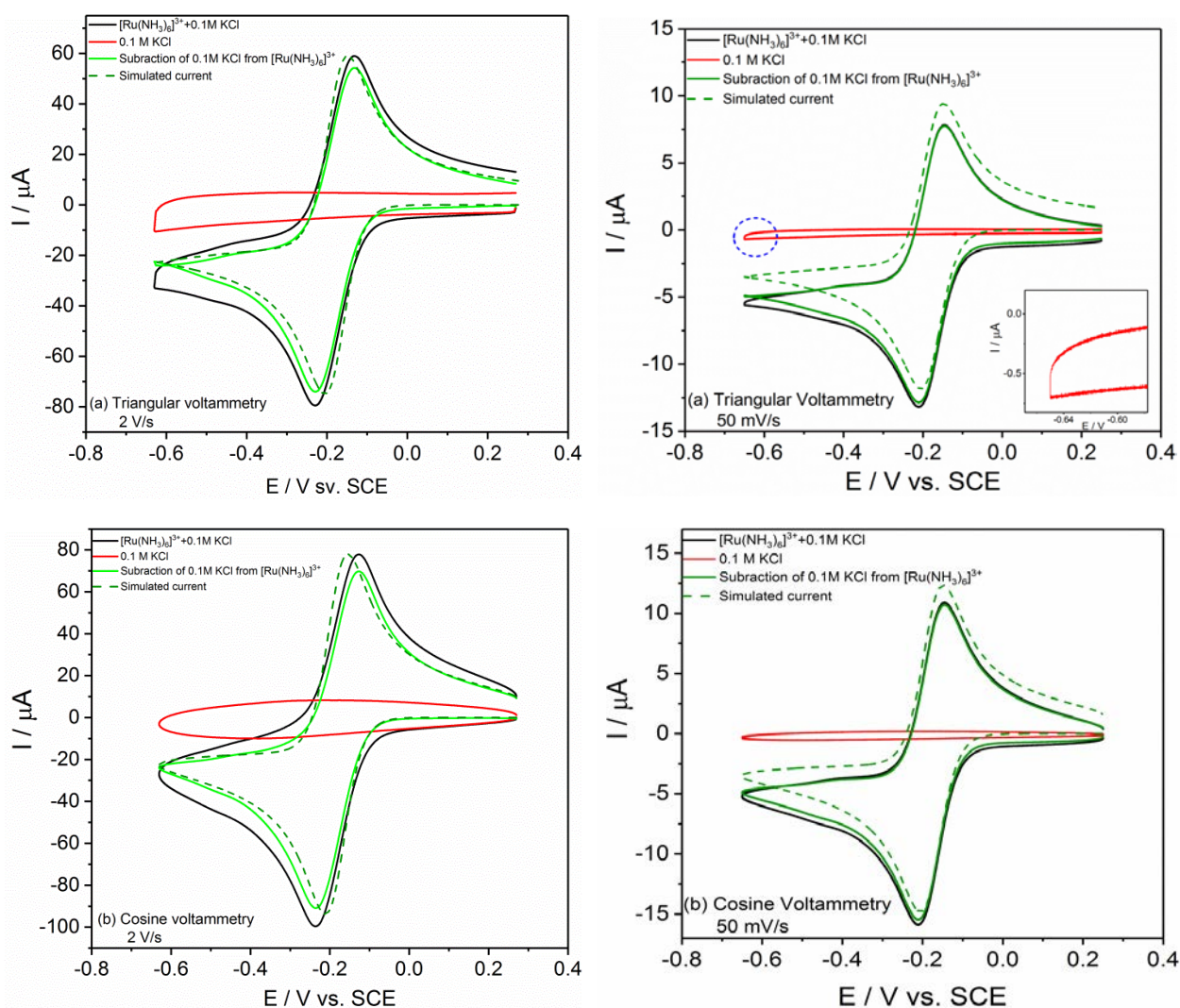
3. Results and Discussion

3.1. Cyclic voltammetry with triangular, cosine and cosine square potential waveforms

First, we address the influence of the suggested waveforms on the capacitive current in blank solutions, and then discuss the voltammetric behaviour of the above mentioned waveforms in $[\text{Ru}(\text{NH}_3)_6]\text{Cl}_3$ solution. Fig. 2 compares the experimental voltammograms obtained in both blank

solution (0.1M KCl) and in 0.96 mM $[\text{Ru}(\text{NH}_3)_6]\text{Cl}_3/0.10 \text{ M KCl}$ solution using the three different waveforms at a scan rate of 2 V s^{-1} : Triangular, cosine and cosine square.

For the triangular wave (red curve), the voltammogram shows a curved-corner rectangle of the capacitive current in the blank solution. At the point of potential reversal (-0.63 V for curves with 2 V s^{-1}), a sharp change in the capacitive current is observed because the current instantly drops upon switching the sweep from forward to backward direction, causing a discontinuity in the voltammogram. On the contrary, the capacitive currents obtained using cosine and cosine square potential waves (given by Eq. (4)) are continuous at all points of the voltammogram as these waves are based on continuous functions, avoiding the current cut at the reversal potential and thus reducing any consecutive influence of the discontinuity on the voltammetric behaviour at high scan rates ($>2 \text{ Vs}^{-1}$).



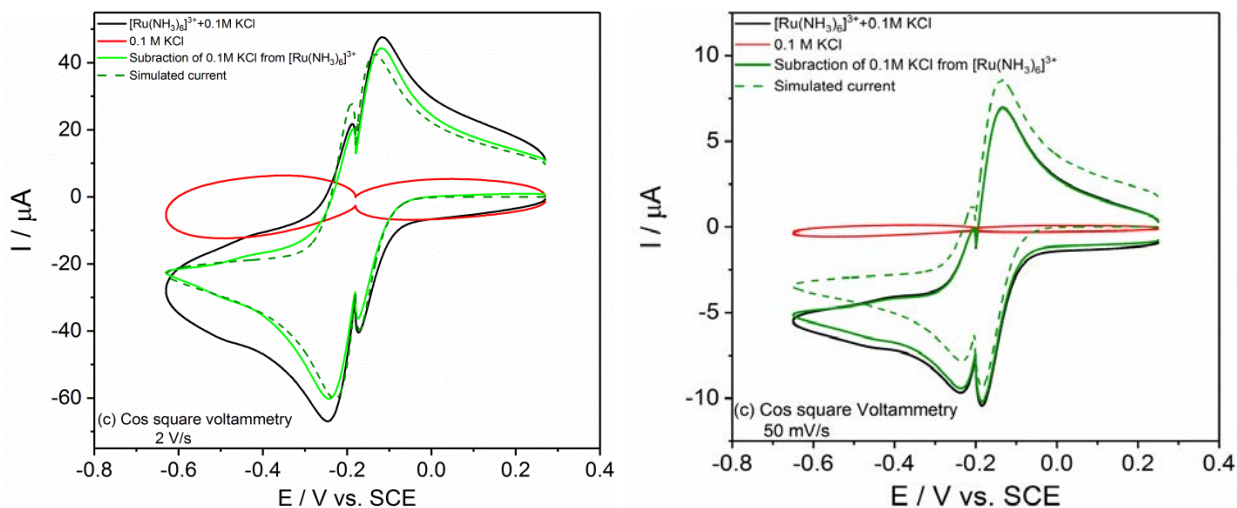


Fig. 2. Voltammograms of (a) triangular, (b) Cosine and (c) cosine square potential waves obtained at GC electrode in blank 0.1 M KCl solution (red curves, capacitive currents) and in 0.96 mM $[\text{Ru}(\text{NH}_3)_6]\text{Cl}_3/0.10$ M KCl solution (black curves, faradaic + capacitive currents) with scan rate of 2 V s^{-1} (left panel) and 0.05 V s^{-1} (right panel). The applied potential window of the curves of the right panel is different by 20 mV from the curves of the left panel. The experimental faradaic-only currents (green curves) are obtained by subtraction. The faradaic simulated currents are shown in the dashed curves.

The voltammetric response of $[\text{Ru}(\text{NH}_3)_6]\text{Cl}_3$ to the applied cosine square potential wave is markedly different from the response to the conventional triangular sweep voltammetry, see Fig. 2a and c: In contrast to the single redox peak of $\text{Ru}^{3+}/\text{Ru}^{2+}$ observed in standard cyclic voltammetry, two distinct peaks are observed at certain value of E_{centre} . However, the cosine potential wave shows a similar voltammogram to the triangular cyclic voltammetry, see Fig. 2b. In all voltammograms, unless otherwise mentioned, the capacitive current was subtracted using blank voltammetry recorded in solutions without the $[\text{Ru}(\text{NH}_3)_6]\text{Cl}_3$ species, and the resulting faradaic-only currents (green solid curves) are also shown.

The voltammograms obtained at a scan rate of 0.05 V s^{-1} are also shown in the right panel of the figure. The split of the signal is also observed for the cosine square wave, and the difference in the shape of the doublet peak between the right panel and the left panel is due to the different applied potential window. This indicates the sensitivity of the peak heights of the two peaks to the applied potential window and in turn E_{centre} . The applied experimental parameters were used to obtain the simulated voltammograms (dashed curves) and the resulting curves are depicted in Fig. 2. The simulated faradaic-only currents are in a very good agreement with the measured faradaic currents. The slight difference in potential between experimental and simulated curves (i.e. quasi-reversible

behaviour) is mostly due to slightly incomplete electrolytic support as discussed previously [17], and slightly due to a delay in the voltage generation.

3.3.3.2. Scan rate dependency of the voltammograms

The scan rate was varied from 0.05 to 2 V s⁻¹ at the same GC electrode in 0.96 mM [Ru(NH₃)₆]Cl₃/0.10 M KCl solution, see Fig. S1. For the cosine-based waves the duration of a single cycle was adjusted such that the average scan rate is the same as that in corresponding triangular cyclic voltammogram. Independent of the applied potential waveform, the measured faradaic current is directly proportional to the square root of scan rate, as shown in Fig. 3. For the reversible one-electron reduction of Ru³⁺, a square root dependency of peak current on scan rate is seen according to Randles-Ševčík equation: [22]

$$I_p = 0.446FAC^o \sqrt{\frac{FDv}{RT}} \quad \text{at 298 K} \quad (7)$$

where I_p is the peak current, D is the diffusion coefficient and C^o is the bulk concentration. Using $D = 8.43 \times 10^{-10} \text{ m}^2 \text{ s}^{-1}$ [18], and $C^o = 0.96 \times 10^{-6} \text{ mol m}^{-3}$, the linear regression of the peak currents obtained from triangular cyclic voltammetry reveals a pre-factor of 0.434 ± 0.001 in Randles-Ševčík equation, which is in a good agreement with the theoretical value of 0.446 (Eq. 7); the error bars of the pre-factors are based on the standard error of the slope. However, for the voltammograms with cosine waveform, the peak currents and consequently the pre-factor in Randles-Ševčík equation are 24% higher than that obtained from the triangular wave, as previously reported from theoretical analysis [15]. This is attributed to the fact that near the formal potential the temporal scan rate for the cosine wave is higher than the corresponding one in the triangular wave, see Fig. 1. For the cosine wave, the modified Randles-Ševčík pre-factor is 0.539 ± 0.001 , which is close to the simulated one of 0.559. Although for the cosine square potential wave the peak is split into two peaks with lower currents, the peak currents are both directly proportional to the square root of scan rate and the modified Randles-Ševčík pre-factors are 0.364 ± 0.0025 for first peak and 0.215 ± 0.003 for the second peak, Fig. 3. The above results confirm that the experimental data for both triangular and cosine waves coincide with the simulation results.

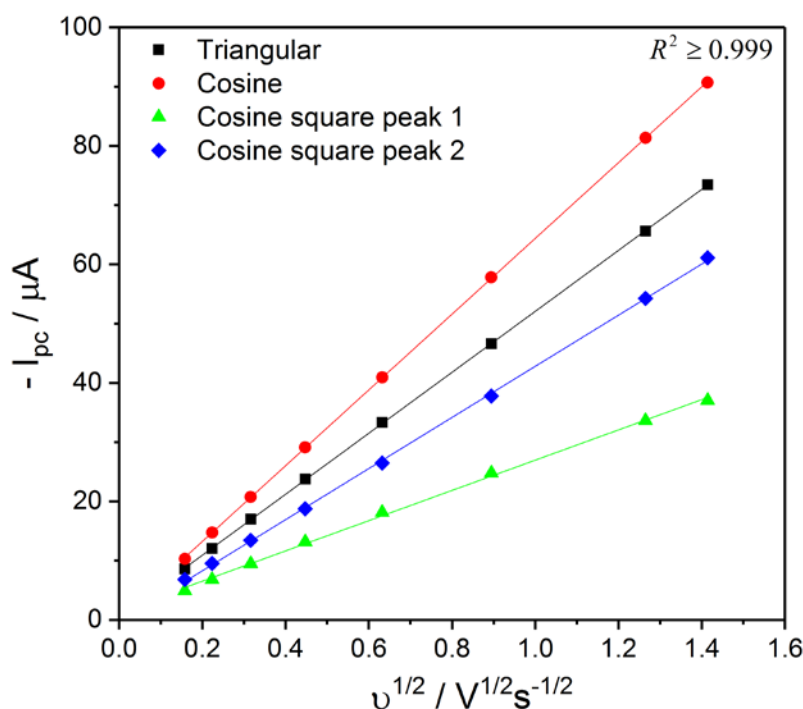


Fig. 3. Plot of cathodic peak currents against the square root of scan rate for the data obtained using triangular, cosine and cosine square potential waves at ranges from 0.05 to 2 V s⁻¹ in 0.96 mM [Ru(NH₃)₆]Cl₃/0.10 M KCl solution at 298 K. The linear regressions are also shown.

3.4.3.3. Analysis of the voltammetric behaviour

To exploit the characteristic features which arise from the cosine square potential wave for quantitative analysis, we applied the cosine square wave given by Eq. (4) using different E_{centre} values by applying different potential windows (i.e. E_{centre} is shifted from -0.05 to -0.35 V in intervals). Examples of the experimental voltammograms are displayed in Fig. 4, and additional voltammograms are presented in the SI. These voltammograms were recorded at the same GC working electrode in 0.96 mM [Ru(NH₃)₆]Cl₃/0.10 M KCl solution at 298 K. The average scan rate is 50 mV s⁻¹, which was achieved by setting the duration of each single cycle to 36 s, as demonstrated in Fig. 1. The same series of voltammograms were recorded for the triangular and cosine potential waveforms. Both waveforms resulted in similar voltammograms with a single peak at the same position independent of the applied potential window (see Fig. S2). In contrast, using the cosine square potential wave the curves have more features, that are exploited for quantitative analysis as discussed below: The single peak is split into a doublet peak at certain E_{centre} values.

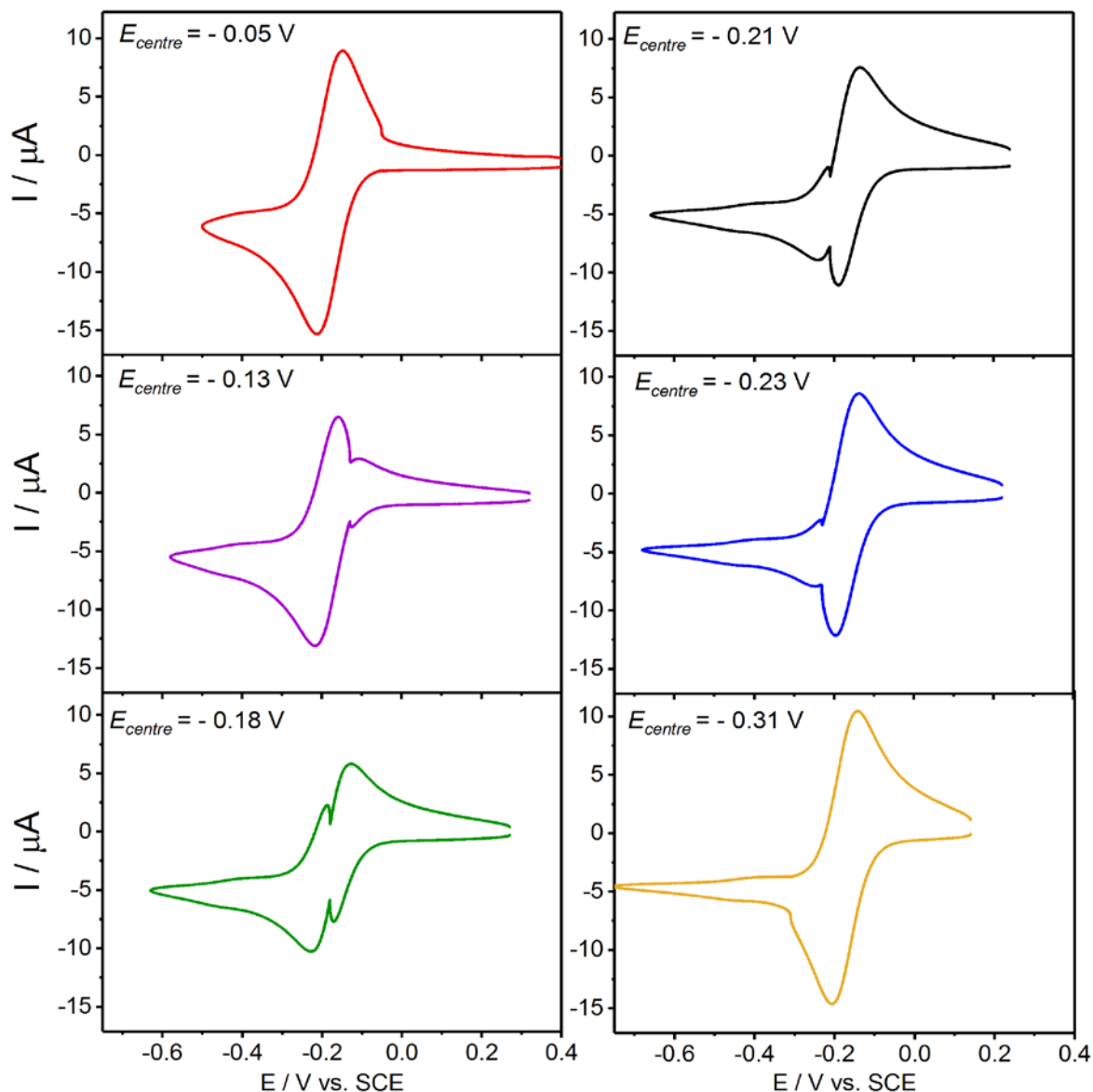


Fig. 4. Capacitive current-corrected voltammograms obtained at GC electrode with the cosine square potential waveform at different E_{centre} values in 0.96 mM $[\text{Ru}(\text{NH}_3)_6]\text{Cl}_3/0.10$ M KCl solution at an average scan rate of 50 mV s^{-1} at 298 K.

To analyse this behaviour, the experimental peak currents are plotted (as points) against the applied E_{centre} (the midpoint potential of the applied potential window) as shown in Fig. 5. Notably, the height of the two peaks varies as E_{centre} is shifted (i.e. the potential window is moved to more positive or negative potentials). At $-0.25 < E_{\text{centre}} < -0.07$ V, the peak splits into two peaks with one peak dominating, and after the point of intersection in the plot the two peaks switch their heights. In contrast, at E_{centre} values lower than -0.25 V the two peaks merge; and at E_{centre} values higher than -0.07 V one peak diminishes. The split of the peak can be clearly explained from the cosine square function (Eq. 4) and its wave shape (Fig. 1): At the midpoint of the potential window, a plateau is observed, which means a temporal hold of potential (i.e. scan rate approaches zero), causing a drop

of current. For direct comparison with theory, we additionally plot the simulated results obtained from the *fractional calculus* method as solid lines (Fig. 5). In our previous theoretical treatment [15], two independent methods, namely the *finite difference* method [19] and the *fractional calculus* method [20] were applied using dimensionless parameters. In this work, we used the dimensional experimental parameters for simulation, and the results of both methods fully agree, see Fig. S3. To this end, the verification of the theory is evident from the excellent agreement with the experimental results.

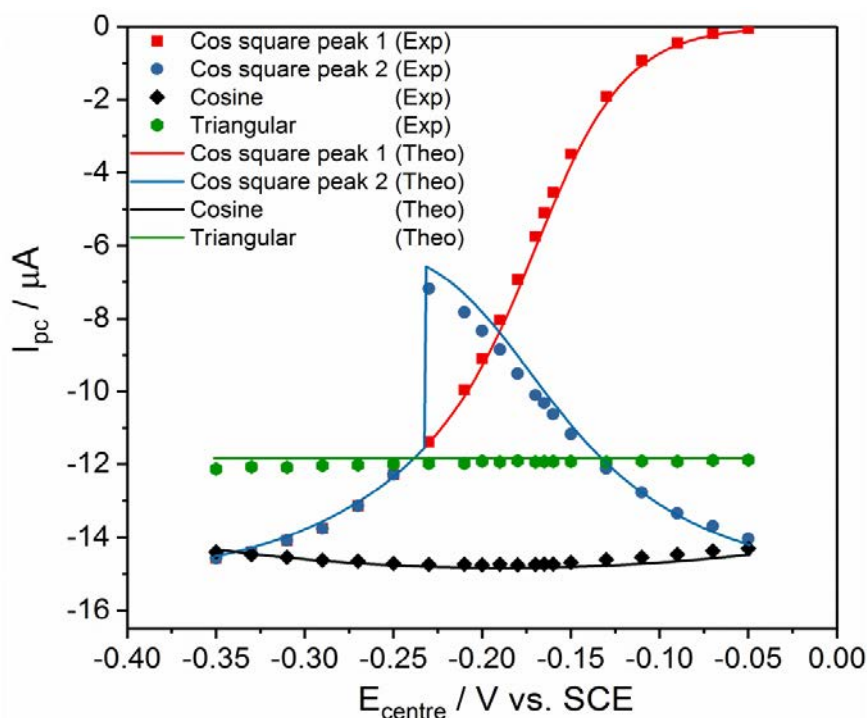


Fig. 5. Plot of the cathodic peak currents (capacitive current-corrected) obtained from the corresponding voltammograms with the triangular, cosine and cosine square waves using different E_{centre} values.

3.5.3.4. Determination of the formal potential of $\text{Ru}[(\text{NH}_3)_6]^{3+/2+}$

A more significant characteristic observed in the voltammetry with the cosine square potential waveform is the strong influence of E_{centre} on the peak-to-peak separation of the voltammogram. As shown in Fig. 6, a drastic change (potential jump) in the peak-to-peak separation appears at a certain E_{centre} values, which is also confirmed in the simulations. The midpoint of this jump in the simulated results best fit the experimental results when a formal potential E_f^0 of -0.175 ± 0.001 V is set in the simulations (i.e. the minimum of this concave step at the jump has the same position in theory and experiment). Thus, E_{centre} value at this minimum denotes the formal potential of the system. Therefore, the peak-to-peak separation in the voltammograms of the cosine square wave provides

an alternative method to determine the formal potential of the $\text{Ru}^{3+}/\text{Ru}^{2+}$ system. For comparison, E_f^o is also determined from the midpoint of the voltammograms with triangular and cosine waves and a value of -0.178 ± 0.001 V is obtained from both methods; the error bars indicate the experimental error of the potentiostat. For further confirmation of the result, an independent experiment with a microelectrode in $[\text{Ru}(\text{NH}_3)_6]\text{Cl}_3$ solution reveals $E_f^o = -0.177 \pm 0.001$ V vs. SCE, see Fig. S5. The E_f^o values obtained from the different methods are consistent to within an experimental error for the analog potentiostat system of ± 1 mV, hence validating our theory. When E_{centre} is far from E_f^o , the peak separation sharply decreases and then approaches the expected value of 57 mV for a reversible one-electron transfer process [3, 23, 24]. For the voltammetry of triangular and cosine waves, the peak-to-peak separation does not change and remains at a value of 64-65 mV, which is also close to the theoretical 57 mV. It is noteworthy to mention that the few millivolts difference from the theoretical value of 57 mV is mostly due to slightly incomplete electrolytic support, and in turn a non-compensated resistance in solution [17]. A ratio of the supporting electrolyte to $[\text{Ru}(\text{NH}_3)_6]\text{Cl}_3$ concentrations of greater than 100 is required to achieve a diffusion only behaviour [17].

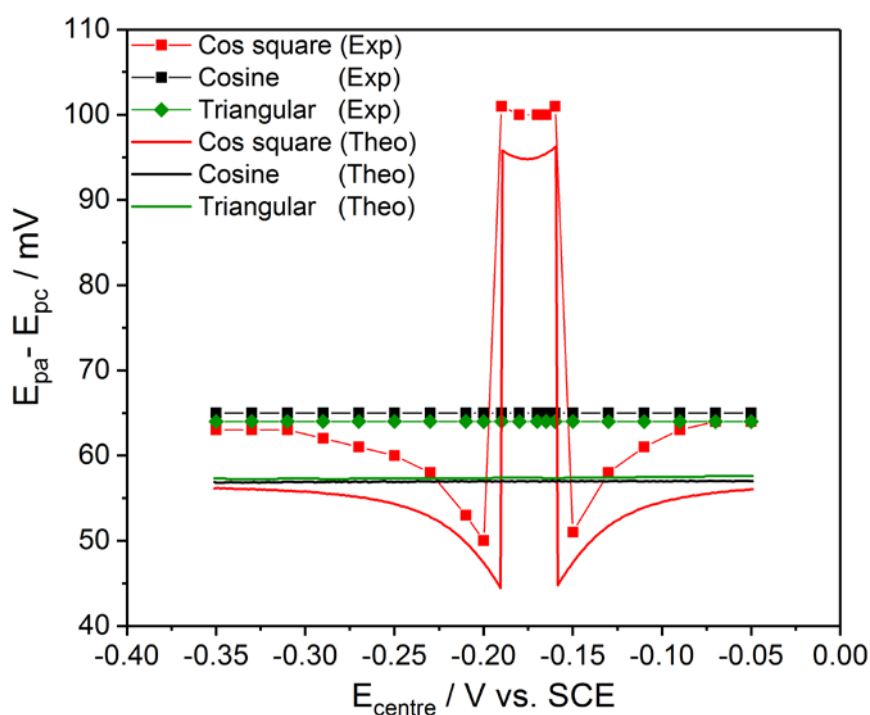


Fig. 5. Plot of the peak-to-peak separation obtained from the corresponding voltammograms with the triangular, cosine and cosine square waves using different E_{centre} values.

4. Conclusions

The theory for a non-triangular potential wave cyclic voltammetry is experimentally verified at macroelectrode for the reversible $\text{Ru}^{3+}/\text{Ru}^{2+}$ system. In contrast to the classical triangular potential wave, a cosine-based potential waveform was employed in cyclic voltammetry to reduce the discontinuity in the capacitive currents at the potential vertex, which inevitably occurs in the triangular cyclic voltammetry. The significant features arise from the voltammograms with cosine square potential wave provided a simple route to determine the formal potential of $\text{Ru}^{3+}/\text{Ru}^{2+}$; and a value of -0.175 V vs. SCE is obtained which agrees with other methods (-0.177 V from microelectrode voltammetry). The verification of the theory is evident from the excellent agreement with the experimental results.

Acknowledgements

H. M. Amin gratefully acknowledges DFG for funding (No. AB 702/1-1). This work is partially funded from the European Research Council under the European Union's Seventh Framework Programme (FP/2007-2013)/ERC Grant Agreement No. 320403. The Authors thank Ms. K. Chaisiwamongkhol for experimental input.

Appendix A. Supplementary Information

Supplementary data to this article can be found online at [...](#)

References

- [1] R.S. Nicholson, I. Shain, Theory of Stationary Electrode Polarography. Single Scan and Cyclic Methods Applied to Reversible, Irreversible, and Kinetic Systems, *Anal. Chem.*, 36 (1964) 706-723.
- [2] A.J. Bard, L.R. Faulkner, *Electrochemical Methods: Fundamentals and Applications*, Wiley, 2001.
- [3] R.G. Compton, C.E. Banks, *Understanding Voltammetry*, 2nd ed., Imperial College Press, 2011.
- [4] F. Marken, A. Neudeck, A.M. Bond, Cyclic Voltammetry, in: F. Scholz (Ed.) *Electroanalytical Methods: Guide to Experiments and Applications*, Springer Berlin Heidelberg, Berlin, Heidelberg, 2002, pp. 51-97.
- [5] H.T.H. Chan, E. Kätelhön, R.G. Compton, Voltammetry at electrodes decorated with an insulating porous film: Understanding the effects of adsorption, *J. Electroanal. Chem.*, 801 (2017) 135-140.
- [6] E. Laviron, L. Roullier, Electrochemical reactions with adsorption of the reactants and electrosorption. Simple analytical solutions for a Henry isotherm, *J. Electroanal. Chem.*, 443 (1998) 195-207.
- [7] C. Amatore, E. Maisonhaute, B. Schöllhorn, J. Wadhawan, Ultrafast Voltammetry for Probing Interfacial Electron Transfer in Molecular Wires, *ChemPhysChem*, 8 (2007) 1321-1329.
- [8] P. Fortgang, C. Amatore, E. Maisonhaute, B. Schöllhorn, Microchip for ultrafast voltammetry, *Electrochem. Commun.*, 12 (2010) 897-900.

- [9] C. Amatore, E. Maisonhaute, When Voltammetry Reaches Nanoseconds, *Anal. Chem.*, 77 (2005) 303 A-311 A.
- [10] C. Amatore, E. Maisonhaute, B. Schöllhorn, Molecular electrochemistry pushed to its limits: from nanosecond kinetics to the dynamic study of nanometric objects, *Actualite Chimique*, (2008) 69-74.
- [11] A. Molina, J. Gonzalez, Pulse Voltammetry in Physical Electrochemistry and Electroanalysis. Theory and Applications, Springer International Publishing, Heidelberg, Germany, 2016.
- [12] F. Scholz, Voltammetric techniques of analysis: the essentials, *ChemTexts*, 1 (2015) 17.
- [13] A.M. Bond, D. Elton, S.-X. Guo, G.F. Kennedy, E. Mashkina, A.N. Simonov, J. Zhang, An integrated instrumental and theoretical approach to quantitative electrode kinetic studies based on large amplitude Fourier transformed a.c. voltammetry: A mini review, *Electrochem. Commun.*, 57 (2015) 78-83.
- [14] E. Laviron, The use of linear potential sweep voltammetry and of a.c. voltammetry for the study of the surface electrochemical reaction of strongly adsorbed systems and of redox modified electrodes, *J. Electroanal. Chem. Interfacial Electrochem.*, 100 (1979) 263-270.
- [15] Y. Uchida, E. Kätelhön, R.G. Compton, Cyclic voltammetry with non-triangular waveforms: Electrochemically reversible systems, *J. Electroanal. Chem.*, 801 (2017) 381-387.
- [16] E. Kätelhön, R.G. Compton, Non-linear sweep voltammetry of adsorbed species: theory and a method to determine formal potentials, *Phys. Chem. Chem. Phys.*, 19 (2017) 28820-28823.
- [17] E.J.F. Dickinson, J.G. Limon-Petersen, N.V. Rees, R.G. Compton, How Much Supporting Electrolyte Is Required to Make a Cyclic Voltammetry Experiment Quantitatively "Diffusional"? A Theoretical and Experimental Investigation, *J. Phys. Chem. C*, 113 (2009) 11157-11171.
- [18] Y. Wang, J.G. Limon-Petersen, R.G. Compton, Measurement of the diffusion coefficients of $[\text{Ru}(\text{NH}_3)_6]^{3+}$ and $[\text{Ru}(\text{NH}_3)_6]^{2+}$ in aqueous solution using microelectrode double potential step chronoamperometry, *J. Electroanal. Chem.*, 652 (2011) 13-17.
- [19] S.W. Feldberg, *Electroanalytical Chemistry*, M. Dekker, New York, 1969.
- [20] K.B. Oldham, J.C. Myland, Modelling cyclic voltammetry without digital simulation, *Electrochim. Acta*, 56 (2011) 10612-10625.
- [21] C. Batchelor-McAuley, J. Ellison, K. Tschulik, P.L. Hurst, R. Boldt, R.G. Compton, In situ nanoparticle sizing with zeptomole sensitivity, *Analyst*, 140 (2015) 5048-5054.
- [22] J.E.B. Randles, A cathode ray polarograph. Part II. - The current-voltage curves, *Transactions of the Faraday Society*, 44 (1948) 327-338.
- [23] A. Molina, J. Gonzalez, M.C. Henstridge, R.G. Compton, Voltammetry of Electrochemically Reversible Systems at Electrodes of Any Geometry: A General, Explicit Analytical Characterization, *J. Phys. Chem. C*, 115 (2011) 4054-4062.
- [24] Z. Ban, E. Kätelhön, R.G. Compton, Voltammetry of porous layers: Staircase vs analog voltammetry, *J. Electroanal. Chem.*, 776 (2016) 25-33.